PLC Channel Characterization up to 300 MHz: Frequency Response and Line Impedance

Fabio Versolatto and Andrea M. Tonello
WiPLi Lab - Università di Udine - Via delle Scienze 208 - 33100 Udine - Italy
e-mail: {fabio.versolatto, tonello}@uniud.it

***Abstract*—We investigate the statistics of the in-home power line communications channel in the broadband frequency range up to 300 MHz. The analysis is based on the results of an experimental measurement campaign in Italy during which we acquired more than 1300 channels.**

Firstly, we focus on the channel frequency response. We study the statistics of the amplitude (in dB). In particular, we infer the normal distribution of the quantity. Furthermore, we examine the statistics of the phase. Then, we study the line impedance. We investigate the statistics of the resistive and reactive component of the line impedance and their relation. Finally, we perform the joint analysis of the line impedance components and the amplitude of the channel frequency response.

I. Introduction

Broadband powerline communication (PLC) exploits the existent power delivery network to deliver high-speed data content and it ensures data rates of up to 200 Mbps at the PHY layer. Recent standardization advances enabled communications beyond 1 Gbps [1]. The performance improvement is the result of optimized MAC mechanisms, multiple-input multiple-output transmission techniques, and the extension of the signalling frequency range.

The idea of using an extended frequency band in PLC is not new. In [2], the use of an impulsive ultra wideband modulation scheme for multi-user PLC communications up to 100 MHz was proposed. PLC up to 100 MHz was discussed also in [3], where it was shown that multicarrier modulation schemes allow for single-input single-output PLC communications up to 1 Gbps. New standards have exploited the benefit provided by the extension of the signalling bandwidth, and they currently enable communications up to 86 MHz (HomePlug AV2).

Further performance improvements can be obtained by signalling beyond 100 MHz. In this respect, a first attempt was presented in [4], where the PLC channel up to 1 GHz was studied both in time and frequency. The work is based on the measurement results on a test bed power line network and it does not provide results for real-life scenarios. Commercial devices were also developed for PLC communications up to 300 MHz [5]. They are based on the MediaXtream solution that is compliant with HomePlug AV in the 2-28 MHz frequency range, and it exploits the 50 - 300 MHz frequency range to improve the data rate. As a result, the maximum data rate approaches 1 Gbps.

In this work, we characterize, from measurements, the PLC channel in the extended frequency range 2 - 300 MHz. We carried out a measurement campaign in Italy, where we collected more than 1300 channel responses in different premises. Some of the results of the measurement campaign were already reported in [6] for the limited frequency range up to 100 MHz.

We provide a time-invariant analysis of the measured data. In this respect, we note that the PLC channel is commonly referred to be linear and periodically time-variant (LPTV), as described in [7]. However, from our experimental observations, we found that the time-dependence is not pronounced in the measurement sites that we considered. Namely, the variation of the channel frequency response (CFR) during the mains period is limited to few dBs.

The work is divided in three parts. Firstly, we characterize the statistics of the CFR both in amplitude and phase, and we compute the maximum achievable rate under the assumption of additive colored Gaussian noise. We measured the power spectral density (PSD) in one of the premises.

Then, we focus on the line impedance. Basically, the line impedance is the load that is seen by the transmitter. In the literature, most of the effort was spent to characterize the narrowband frequency range, i.e., below 500 kHz, where the line impedance exhibits very low values, with peaks that rarely exceed 60 Ω [8]. In the broadband frequency range, the variation in frequency is more pronounced and the line impedance may vary from few to thousands of Ohms. From measurements, we characterize the real and the imaginary part of the line impedance as a function of the frequency in the 2 - 300 MHz frequency band. The analysis is provided in statistical terms.

Finally, we study the relation between the line impedance and the CFR. In [8], a similar analysis was provided for the 50-500 kHz frequency range. However, at the best of our knowledge, the joint characterization of the quantities has never been presented for the broadband frequency range.

The structure of the paper is as follows. In Section II, we provide details on the measurement campaign. In Section III, IV and V we characterize the CFR, the line impedance, and the relation between the two quantities, respectively. Finally, some conclusions follow.

II. Measurement Campaign

We performed measurements in three Italian premises that are representative of small flats and detached houses of the urban and suburban scenario. For each site, we assessed the channel between all the couples of outlets were no loads where

978-1-4673-0921-9/12/$31.00 ©2012 IEEE

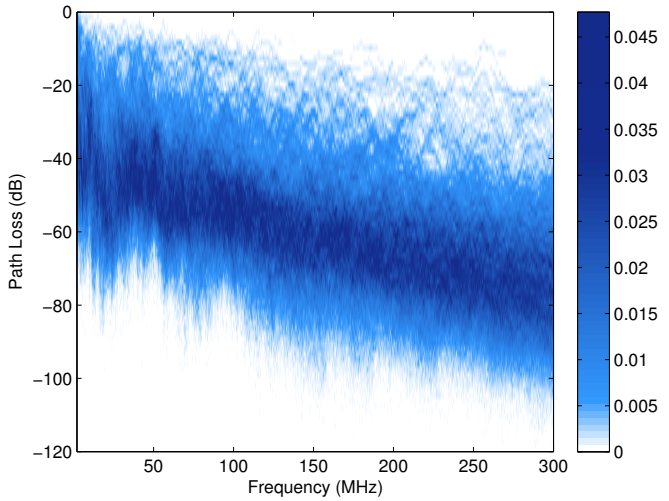

Fig. 1. Probability density function (PDF) of the path loss.

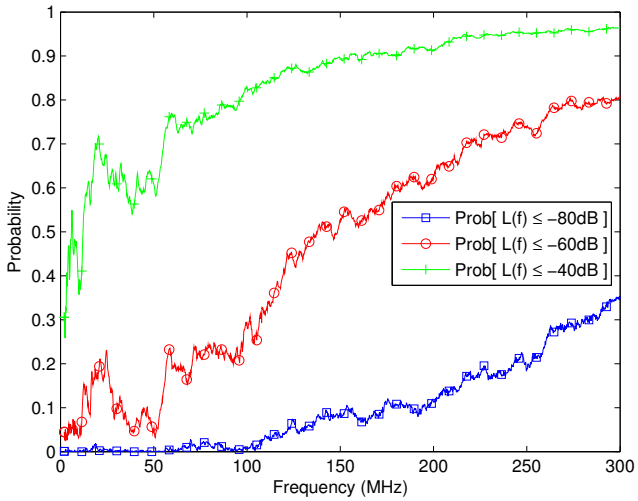

Fig. 2. Probability of the path loss to fall below -40, -60 and -80 dB as a function of the frequency.

connected. We note that we did not remove the appliances that were already connected.

We performed measurements in the frequency domain. Basically, we acquired the scattering parameters (s-parameters) with a vector network analyzer (VNA). We let the transmit power be 10 dBm and, for each channel measure, we averaged 16 acquisitions to obtain the actual s-parameters. From experimental evidences, we observed that 16 acquisitions were sufficient to cope with noise and to provide an average characterization of the channel. We connected the VNA to the network through coaxial cables and broadband couplers. Couplers protect the equipment from the mains and they show an attenuation of 50 dB at the mains frequency, lower than 5 dB up to 100 MHz, and between 5 and 10 dB from 100 to 300 MHz. The measures are reliable for channel responses having attenuation up to 100 dB.

We calibrated the VNA when only the cables were connected and we removed the effect of the couplers by exploiting the chain rule of the ABCD matrices. To this aim, we characterized the couplers in terms of ABCD matrices. The procedure proved to be the most reliable.

The final result is the 2×2 s-parameter matrix $\mathbf{S}(f)$ of the measured channel. From $\mathbf{S}(f)$, we obtain the CFR and the line impedance. We define the CFR as the ratio between the voltage at the receiver port and the voltage at the transmitter port. Further, we define the line impedance as the ratio between the voltage and the current at the transmitter port. We denote the CFR and the line impedance with $H(f)$ and $Z(f)$, respectively. The CFR from the transmitter to the receiver port is not identical to that on the opposite direction [9]. Of course, the symmetry holds for the ratio between the voltage at the receiver port and the source voltage, under the assumption that the load impedance and the source internal impedance are equal in value. We collected more than 1300 CFRs and line impedances. In the following, we identify the m-th link with the apix $\{\cdot\}^{(m)}$, where $m = 1, \ldots, \mathcal{M}$ and $\mathcal{M} = 1312$.

The VNA acquires a finite number of samples. Therefore, we use a discrete-frequency representation. The resolution in frequency Δf is equal to 187.5 kHz. Furthermore, the start and the stop frequency are equal to $f_1 = N_1 \Delta f = 2.06$ MHz and $f_2 = N_2 \Delta_f = 300$ MHz, respectively. From now on, we use the compact notation $n = N_1, \ldots, N_2$ to indicate the n-th frequency sample, i.e., $f = n\Delta f$.

III. Channel Frequency Response

Firstly, we study the statistics of the amplitude of the CFR. From measurements, we compute the probability density function (PDF) of $L(n) = 10 \log_{10} |H(n)|^2$. In the following, we refer to $L(n)$ as path loss and we approximate the PDF of $L(n)$ with the histogram of the values obtained from measurements. In Fig. 1, we show the results. The PDF is a function of the frequency and it is well-confined in a range of 40 dB. We denote with $L_M(n)$ the path loss value that corresponds to the highest PDF value at the n-th frequency sample. From measurements, we have found that $L_M(n)$ is well fitted by the following relation

$$L_M(n) = 3.91 \cdot 10^{-6} n^2 - 0.03n - 42.0311 \quad [dB], \qquad (1)$$

where $n = N_1, \ldots, N_2$. From the PDF, we compute the probability that $L(n)$ is lower than or equal to -40, -60 and -80 dB. In Fig. 2, we show the results. Beyond 100 MHz, the attenuation is greater than 40 dB in more than 80% of the cases. However, the noise PSD is lower as well. It follows that signalling above 100 MHz turns into an achievable rate improvement, as shown in Section III-A.

Now, we investigate the normality of $L(n)$. In the literature, it has been said that the PLC channel is affected by shadow fading. The shadow fading implies a normal distribution of the path loss. In this respect, we perform the Jarque-Bera, Lillieforse and Kolmogorov-Smirnov tests to verify the normality of the measured path losses. In Fig. 3, we show the

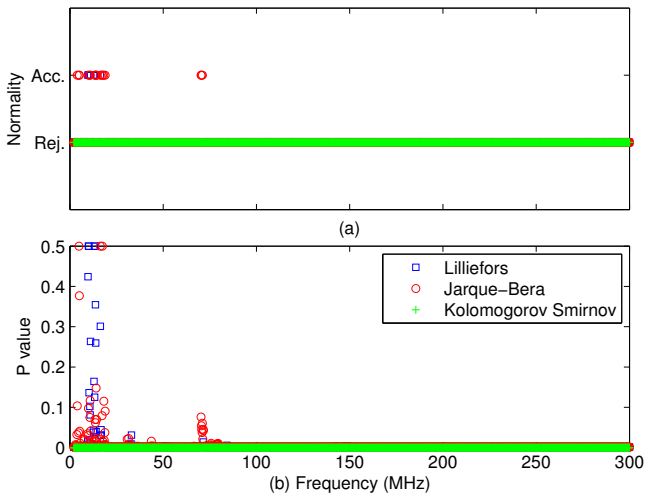

Fig. 3. Results of the normality tests for the path loss.

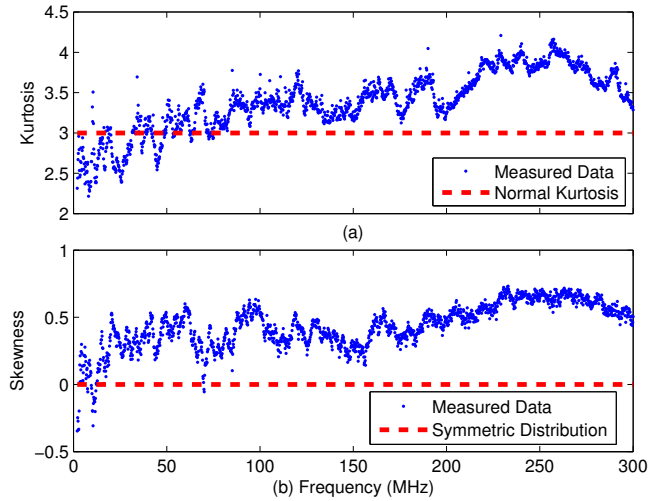

Fig. 4. Statistical characterization of the path loss. On top, the kurtosis. On bottom, the skewness.

results. Basically, in Fig. 3a, we report the frequencies where the null hypotesis is accepted or rejected. When the null-hypotesis is accepted the tests confirm the normality of the measured distribution. In Fig. 3b, we show the correspondent p-value. The higher the p-value, the higher the probability that the measured distribution is normal and deviations are amenable to random errors.

Tests do not strictly confirm the normality. In detail, the Kolmogorov-Smirnov rejects always the null hypotesis, and Jarque-Bera and Lilliefors tests highlight a normal behavior only for few frequency samples below 25 MHz. Deviations from normality are due to the tails of the measured distribution.

To quantify deviations, we study the kurtosis and the skewness of the measured distribution. A similar analysis was previously reported in [10] for the frequency range up to 30 MHz. In Fig. 4a, we show the kurtosis, that is defined as follows

$$K(n) = \frac{E_m\left[(L^{(m)}(n) - \mu_L(n))^4\right]}{\sigma_L^4(f)}, \tag{2}$$

where $E_m[\cdot]$ denotes the average in m, and $\mu_L(n)$ and $\sigma_L(n)$ are the mean and the standard deviation of $L(n)$, respectively. The kurtosis is a scalar metric that is representative of the shape of the measured distribution. The kurtosis of the normal distribution is 3. From Fig. 4a, we note that the kurtosis of the measured path loss is close to 3 for most of frequencies. Therefore, the kurtosis of the measured distribution is not significantly different from the normal one. In Fig. 4b, we show the skewness. Similarly to the kurtosis, the skewness is defined as follows

$$S(n) = \frac{E_m\left[(L^{(m)}(n) - \mu_L(n))^3\right]}{\sigma_L^3(n)}, \tag{3}$$

and it describes the symmetry of the distribution $L(n)$. When $S(n)$ is zero, the distribution is symmetric. From Fig. 4b, we note that the measured distribution is not symmetric because the skewness is larger than 0 for most of frequencies.

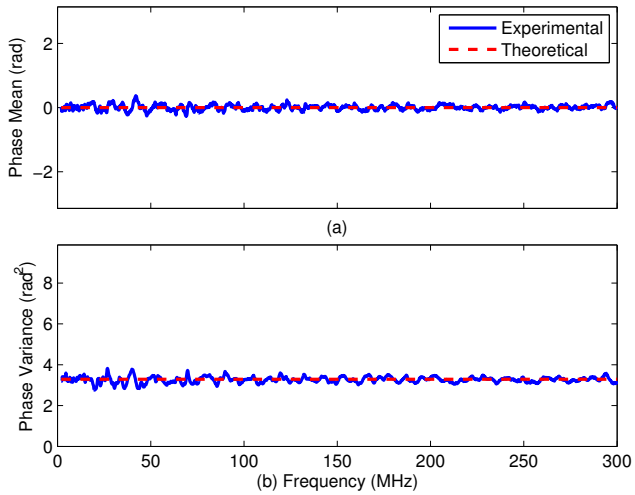

Fig. 5. Mean (on top) and variance (on bottom) of the phase of the CFR.

We compared the measured distribution to other well-known distributions. From the comparison, the normal distribution provides the best matching. Therefore, the normal distribution is still the best fit, though it is not strictly confirmed by the statistical tests.

Now, we study the statistics of the phase $\phi^{(m)}(n) = \angle H^{(m)}(n)$. The phase of the measured channels can be modelled as a uniformly distributed random variable in $(-\pi, \pi)$. In Fig. 5, we report the mean and the variance of the phase. As it can be noted, the mean and variance of the measured phase are close to the theoretical mean and variance of a uniformly distributed random variable in $(-\pi, \pi)$ (red dashed lines).

A. Achievable Rate Improvement

We aim to investigate the improvement provided by the extension of the signalling band up to 300 MHz. We focus on the achievable rate. We assume the transmitted signal to be normally distributed and the transmission to be affected by

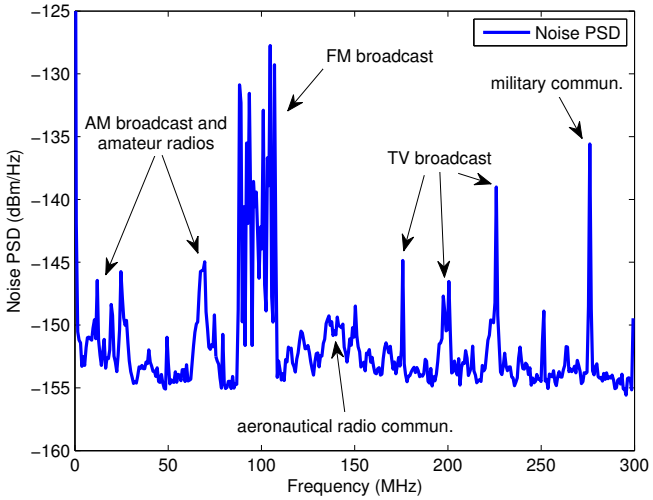

Fig. 6. PSD of the measured background noise. The noise disturbances above -150 dBm/Hz are also described.

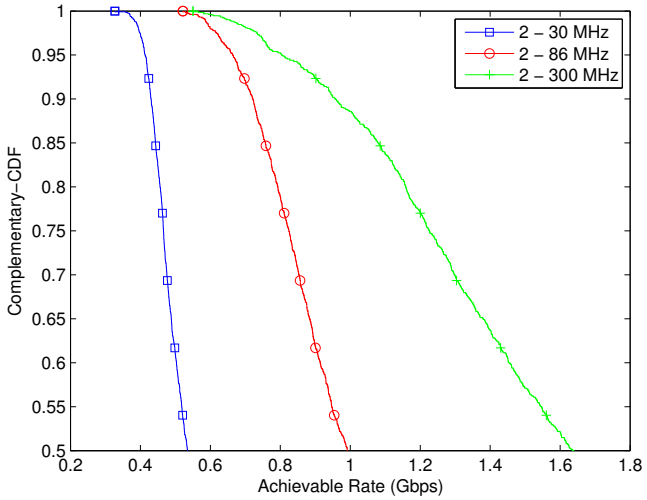

Fig. 7. Complementary cumulative distribution function of the achievable rate for three different transmission bands.

additive colored Gaussian noise. We neglect the impact of the impulsive noise. The achievable rate reads as follows

$$C^{(m)} = \Delta f \sum_{n=N_1}^{N_2} \log_2 \left(1 + \frac{|H^{(m)}(n)|^2 P_{tx}(n)}{P_w(n)}\right) \quad [bps], \tag{4}$$

where $P_{tx}(n)$ and $P_w(n)$ are the PSD of the transmitted signal and the noise, respectively. We let $P_{tx}(n)$ be 10^{-5} mW/Hz up to 30 MHz, and 10^{-8} mW/Hz otherwise. The latter value enables satisfying CISPR requirements on radiated emissions [11]. Concerning the noise, we model $P_w(n)$ according to measurements. With a spectrum analyzer, we acquired the PSD of the background noise in one of the measurement sites. In Fig. 6, we show the measured PSD profile in dBm/Hz. Basically, we experienced a noise floor of -155 dBm/Hz and several narrowband noise interferences. FM broadcast radios are the dominant ones. They increase the noise PSD of up to 25 dB. However, other narrowband interferences are present. In Fig. 6, we also describe the possible interference sources that lead to noise spikes, according to the Italian regulations on spectrum allocation.

We consider three different transmission bands, namely, 2-30 MHz, 2-86 MHz, and 2-300 MHz, and we denote them with B_1, B_2 and B_3, respectively. We remark that 86 MHz is the stop transmission frequency of HomePlug AV2 [1]. In Fig. 7, we show the complementary cumulative distribution function (C-CDF) of the achievable rate for all the three cases. We limit the plot to the values of the C-CDF that are greater than 0.5. In 80% of the cases, the achievable rate is greater than 456 Mbps, 793 Mbps, and 1.16 Gbps for transmissions in B_1, B_2 and B_3, respectively. We note that these values are quite high, as a consequence of the low level of the noise PSD that we measured and that is approximately -155 dBm/Hz except for the bands impaired by narrowband interferers. In Tab. I, we report the mean, average and maximum value of C for three transmission bands. Interestingly, the average increase of the achievable rate is not proportional to the increase of the transmission bandwidth. In this respect, we compute the average spectral efficiency η. We define the average spectral efficiency as the ratio between the average value of C and the correspondent transmission bandwidth. From B_1 to B_2 and B_3 the spectral efficiency decreases by a factor 2/3 and 1/3, respectively.

TABLE I
MINIMUM, MEAN AND MAXIMUM ACHIEVABLE RATE VALUES, AND MEAN SPECTRAL EFFICIENCY FOR THE THREE TRANSMISSION BANDS

Band (MHz)	min$\{C\}$ (Mbps)	mean$\{C\}$ (Mbps)	max$\{C\}$ (Gbps)	η (bps/Hz)
2 - 30	327	555	0.89	19.8
2 - 86	522	1062	2.08	12.6
2 - 300	551	1930	6.13	6.5

IV. Line Impedance

We now carry out a statistical analysis of both the real and the imaginary part of the line impedance. We denote the real (resistive) and imaginary (reactive) component of the line impedance at n-th frequency sample with $R(n)$ and $X(n)$, respectively. In Fig. 8, we show the PDF of $R(n)$ and $X(n)$ as a function of the frequency. Basically, we compute the PDF as the histogram of the measured values of the line impedance. On the x-axis, we report the frequency values, on the y-axis, we report the resistive (Fig. 8a) and reactive (Fig. 8b) component values. White-colored areas indicate zero-probability regions. For clarity, we magnify the plot to the areas that correspond to the higher probability values. Concerning the resistive component, we note that, it is more spread in the lower frequency range and, beyond 150 MHz, the high-probability area is concentrated below 40 Ω. Indeed, the PDF of the reactive component is well-confined in the positive-value region between 0 and 100 Ω. Further, it shows

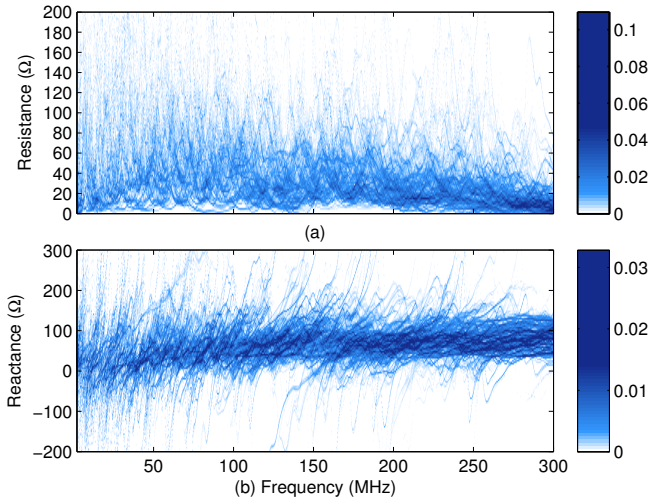

Fig. 8. PDF of the resistive (on top) and reactive (on bottom) component of the measured line impedances.

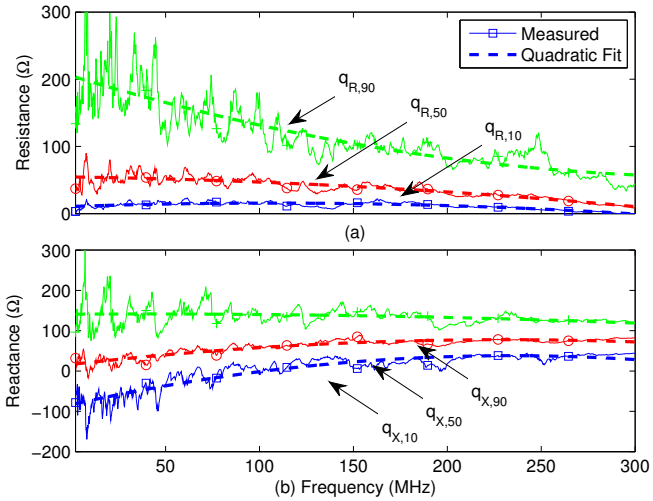

Fig. 9. Quantiles of the resistive (on top) and reactive (on bottom) component of the line impedance. Three probability values are considered, i.e., 10, 50 and 90%, and the quadratic fit is also shown (dashed lines).

a frequency-increasing behavior. It follows the inductive-like behavior of the PLC channel.

In order to provide a first analytical attempt to describe the statistics of the line impedance, we study the cumulative distribution function of $R(n)$ and $X(n)$. A similar characterization for the narrowband frequency range was presented in [8]. We focus on the quantiles $q_{\Lambda,\alpha}(n)$ of the probability function $P\left[\Lambda(n) \leq q_{\Lambda,\alpha}(n)\right] = \alpha$, where $\Lambda \in \{R, X\}$. We consider three probability values, i.e., $\alpha = 10$, 50 and 90 %, and, in Fig. 9, we show the profiles as a function of the frequency. We perform the quadratic fitting of the quantile profiles as

$$\hat{q}_{\Lambda,\alpha}(n) = a_{\Lambda,\alpha} n^2 + b_{\Lambda,\alpha} n + c_{\Lambda,\alpha} \quad [\Omega]. \tag{5}$$

where $\Lambda = R, X$, $\alpha = 10, 50, 90$ and $n = N_1, \ldots, N_2$. In Table II, we collect the values of the constant coefficients $a_{\Lambda,\alpha}$, $b_{\Lambda,\alpha}$ and $c_{\Lambda,\alpha}$. For clarity, we also show the quadratic fitting profiles in Fig. 9. The analytical expression in (5) is useful to quantify both the compression of $R(n)$ toward the lower values in the higher frequency range and the frequency-increasing behavior of $X(n)$.

Finally, we study the correlation between the resistive and the reactive component of the line impedance. In Fig. 10, we show the scatter plot of the samples $\left(X^{(m)}(n), R^{(m)}(n)\right)$, where $n = N_1, \ldots, N_2$ and $m = 1, \ldots, \mathcal{M}$. We use the logarithmic scale for the resistive component in order to characterize with high accuracy the range of lower values, i.e., below 10 Ω. Interestingly, we note the followings. First, the resistance is upper-limited to 3.4 $k\Omega$ and the reactance ranges between 1.9 and -1.7 $k\Omega$. Second, high reactive values correspond to high resistive values. Third, when the resistive component is low, say, below the unit, the reactance is positive and approximately equal to 121 Ω.

TABLE II
QUADRATIC FITTING PARAMETER VALUES

Λ	α	$a_{\Lambda,\alpha}$ (Ω)	$b_{\Lambda,\alpha}$ (Ω)	$c_{\Lambda,\alpha}$(Ω)
R	10	-1.52408e-005	0.0173875	10.6255
	50	-1.24862e-005	-0.007603	54.497
	90	4.22908e-005	-0.15971	204.808
X	10	-7.7903e-005	0.194246	-83.0237
	50	-4.03536e-005	0.099447	16.4242
	90	-1.16296e-005	0.00486855	140.98

V. Connections between the line Impedance and the Path Loss

In Fig. 11, we show the scatter plot of both the resistive and the reactive component of the line impedance as a function of the path loss, i.e., $\left(L^{(m)}(n), R^{(m)}(n)\right)$ and $\left(L^{(m)}(n), X^{(m)}(n)\right)$, where $N_1 \leq n \leq N_2$ and $m = 1, \ldots, \mathcal{M}$.

We identify a high-density area to which 98% of the measured samples belong. From the experimental evidence, we shape the border of the high-density area as an ellipse that we describe as follows

$$\frac{(\ell - m_\ell)^2}{u^2} + \frac{(z - m_z)^2}{w^2} = 1, \tag{6}$$

where ℓ and z are the path loss, and the line impedance component, respectively, and all other terms are constant coefficients. We model m_ℓ as the expected value of the measured path loss samples, i.e., $m_\ell = E_{m,n}[L^{(m)}(n)] = -57.58$ dB, where $E_{m,n}[\cdot]$ denotes the average in m and n. Now, we focus on the resistance. For the resistance, $z = \log_{10}(R)$, $m_z = E_{m,n}[\log_{10}(R^{(m)}(n))] = 1.44$, and the values of the remaining constant coefficients that describe the high-density area are $u = 54.05$ and $w = 1.54$. Finally, for the reactance, $z = X$, $m_z = E_{m,n}[X^{(m)}(n)] = 66.73$, $u = 54.05$, and

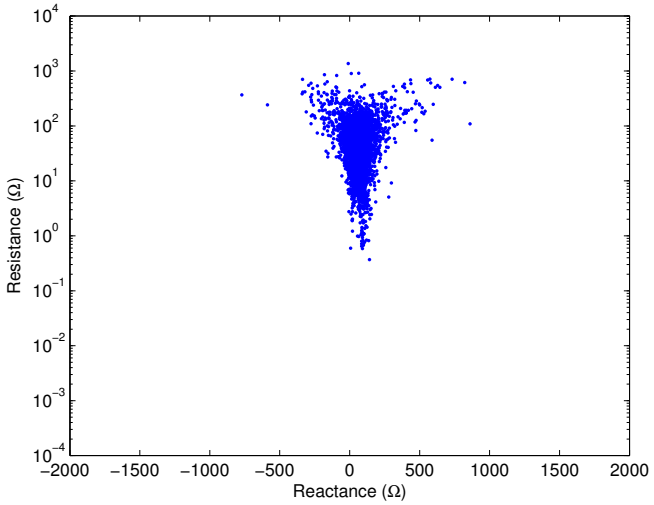

Fig. 10. Scatter plot of the resistance versus the reactance component of the line impedance.

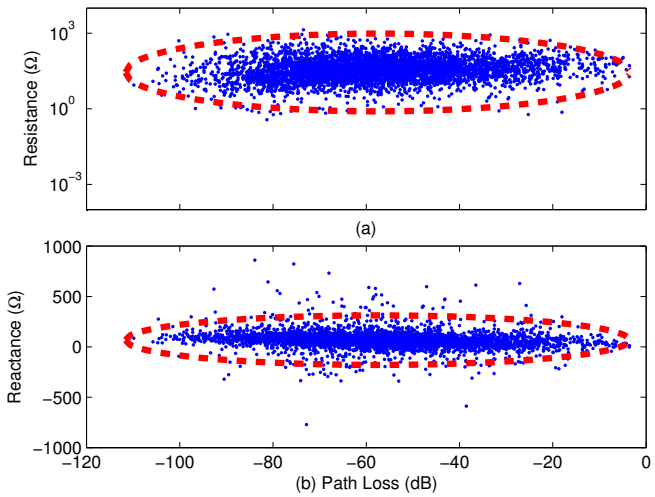

Fig. 11. Scatter plot of the resistive (on top) and the reactive (on bottom) component of the line impedance versus the path loss. The high-density areas are also shown.

$w = 245.58$. Again, we use the logarithmic scale for the resistance to magnify the range of lower value.

VI. Conclusions

We have presented the statistical characterization of the PLC channel from the results of an experimental measurement campaign that we have performed in Italy, where we have collected more than 1300 channel responses.

Firstly, we have studied the channel frequency response (CFR). We have focused on the amplitude in dB, namely, the path loss. We have performed several normality tests and we have investigated the kurtosis and the skewness. Results do not confirm the normality of the path loss, though the normal distribution is the best fit. Concerning the phase, we have found that it is uniformly distributed, and we have reported its mean and variance as a function of the frequency. Furthermore, we have inferred the performance improvement provided by the band extension. We have presented the results in terms of achievable rate for a measured noise profile. We have shown that the achievable rate increases, but the spectral efficiency, i.e., the bitrate per unit frequency, decreases significantly.

Then, we have addressed the statistics of both the real (resistive) and the imaginary (reactive) component of the line impedance. Basically, we have noted the following. First, the resistive component is compressed toward the lower values in the higher frequency range. Second, for most of the frequencies, the reactive component is positive and frequency increasing. Therefore, the measured channels exhibit an inductive-like behavior. Furthermore, we have investigated the relation between the components, and we have found that low resistive values correspond to low reactive values.

Finally, we have studied the relation between the line impedance components and the path loss. No simple relation has been found. Rather, we have identified high-probability regions.

References

[1] Home Plug AV2. [Online]. Available: https://www.homeplug.org/tech/av2/

[2] A. M. Tonello, "Wideband Impulse Modulation and Receiver Algorithms for Multiuser Power Line Communications," *EURASIP Journal on Advances in Signal Processing*, vol. 2007, pp. 1–14.

[3] A. M. Tonello, P. Siohan, A. Zeddam, and X. Mongaboure, "Challenges for 1 Gbps power line communications in home networks," in *proc. IEEE Int. Symp. Personal, Indoor and Mobile Radio Commun. (PIMRC)*, Sep. 2008, pp. 1–6.

[4] S. Chen, X. Chen, and C. Parini, "Measurement and Simulation of Powerline Channel using OFDM for UWB Communication," in *Proc. Int. Symp. on Power Line Commun. and Its App. (ISPLC)*, Mar 2009, pp. 79–84.

[5] Solwise, 1 Gbps powerline adapter. [Online]. Available: http://www.solwise.co.uk

[6] F. Versolatto and A. M. Tonello, "On the Relation Between Geometrical Distance and Channel Statistics in In-Home PLC Networks," in *Proc. Int. Symp. on Power Line Commun. and Its App. (ISPLC)*, Mar 2012, pp. 280–285.

[7] F. J. Cañete, J. A. Cortés, L. Díez, and J. T. Entrambasaguas, "Analysis of the Cyclic Short-Term Variation of Indoor Power Line Channels," *IEEE Journal on Selected Areas in Communications*, vol. 24, no. 7, pp. 1327–1338, Jul. 2006.

[8] J. Bausch, T. Kistner, M. Babic, and K. Dostert, "Characteristics of Indoor Power Line Channels in the Frequency Range 50 - 500 kHz," in *Proc. Int. Symp. on Power Line Commun. and Its App. (ISPLC)*, Mar 2006, pp. 86–91.

[9] T. C. Banwell and S. Galli, "On the Symmetry of the Power Line," in *Proc. IEEE Int. Symp. Power Line Commun. and Its App. (ISPLC)*, Apr. 2001, pp. 325–330.

[10] S. Galli, "A Simple Two-Tap Statistical Model for the Power Line Channel," in *Proc. Int. Symp. on Power Line Commun. and Its App. (ISPLC)*, Mar 2010, pp. 242–248.

[11] B. Praho, M. Tlich, P. Pagani, A. Zeddam, and F. Nouvel, "Cognitive Detection Method of Radio Frequencies on Power Line Networks," in *Proc. IEEE Int. Symp. Power Line Commun. and Its App. (ISPLC)*, Apr. 2010, pp. 225–230.